Building and Environment 205 (2021) 108249

Contents lists available at ScienceDirect

Building and Environment

journal homepage: www.elsevier.com/locate/buildenv

Real-time measurements of fluorescent aerosol particles in a living laboratory office under variable human occupancy and ventilation conditions

Satya S. Patra [a,b], Tianren Wu [a,b], Danielle N. Wagner [a,b], Jinglin Jiang [a,b], Brandon E. Boor [a,b,*]

[a] Lyles School of Civil Engineering, Purdue University, West Lafayette, IN, USA
[b] Ray W. Herrick Laboratories, Center for High Performance Buildings, Purdue University, West Lafayette, IN, USA

ARTICLE INFO

Keywords:
Indoor air quality
Bioaerosols
Laser-induced fluorescence (LIF)
Building ventilation
Indoor microbiology

ABSTRACT

The abundance of super-micron biological and abiotic particles in occupied indoor environments can be influenced by time-dependent changes in human-associated emissions and building ventilation conditions. Real-time measurements of fluorescent aerosol particles (FAPs) were integrated with a building sensing platform to evaluate the influence of human occupancy and ventilation on the temporal dynamics of fluorescent biological and abiotic particles in a living laboratory office. Concentrations and size distributions of FAPs were measured via laser-induced fluorescence (LIF). Human occupants were identified as a major source of super-micron FAPs in mechanically ventilated office buildings. Mass concentrations and size distributions of FAPs larger than 3 μm scaled with human occupancy in the office. Detailed single particle fluorescence data indicated that human-associated emissions enriched the office atmosphere with specific FAP types that varied in morphology. Office occupants were strong emitters of ABC-type particles (number and mass), and to a lesser extent, A-type particles (number and mass), AB-type particles (mass), and B-type particles (mass). Such FAP types are related to common indoor bacterial and fungal aerosols and fluorescent clothing fabric fibers. The introduction of natural ventilation via a double skin glass façade increased the indoor abundance of FAPs due to the efficient transport of outdoor FAPs into the office. While LIF provides valuable real-time data on indoor FAP dynamics, it lacks specificity and cannot fully resolve the origins of fluorescent biological and abiotic particles in indoor spaces.

1. Introduction

Human occupants are a major source of super-micron biological and abiotic particles in indoor environments. Human-associated emissions include the release of super-micron particles from the human envelope (skin, hair, clothing, exhaled breath) and human movement-induced particle resuspension from indoor surfaces [1–20]. Such processes can significantly increase coarse mode particle mass concentrations in occupied spaces in residential and office buildings [21]. Primary emissions of biological particles from the human envelope include bacterial and fungal aerosols associated with the microbiota of the skin, hair, and oral/nasal cavities; viral aerosols produced by respiratory activities; and skin cells and fragments [22–33]. Clothing acts as a primary source of abiotic particles, such as clothing fabric fibers, and as a secondary source of biological and abiotic particles that collect on clothing over time [13,14]. Human-driven particle resuspension from flooring and furniture surfaces can release the biological and abiotic content of settled dust into indoor air [21].

The transient nature of human occupancy patterns in residential and office buildings is expected to drive time-dependent changes in the concentrations of human-emitted super-micron particles. Studies have identified temporal relationships between the presence of humans and the abundance of airborne bacterial and fungal aerosols [1,14,29,34,35]. Occupancy can change rapidly, from seconds to minutes to hours, in indoor environments such as collaborative open-plan offices, classrooms, and other public spaces [36]. The operation of building heating, ventilation, and air conditioning (HVAC) systems can also influence concentrations of indoor-generated particles. Similar to occupancy, their operational modes change over variable time-scales [37,38]. Coupled, real-time measurements of super-micron particles, human occupancy, and building ventilation are therefore needed to understand the factors that modulate airborne populations of human-emitted

* Corresponding author. Lyles School of Civil Engineering, Purdue University, West Lafayette, IN, USA.
E-mail address: bboor@purdue.edu (B.E. Boor).

https://doi.org/10.1016/j.buildenv.2021.108249
Received 21 May 2021; Received in revised form 2 August 2021; Accepted 9 August 2021
Available online 11 August 2021

biological and abiotic particles in dynamic and densely occupied indoor spaces.

Laser-induced fluorescence (LIF) techniques offer a basis to detect fluorescent biological and abiotic particles of human origin in real-time (1 Hz). LIF-based aerosol instruments can provide useful time-resolved data on concentrations and size distributions of human-associated fluorescent aerosol particles (FAPs) that cannot be captured through offline measurement techniques that lack high time-resolution [39–44]. LIF classifies particles by their fluorescence properties, providing a basis to identify specific types of biological and abiotic particles [45,46]. Measurement campaigns involving LIF-based instrumentation have been conducted in outdoor environments [47–52] and selected indoor environments [53–57], including two short-term (<1 week) campaigns in office spaces [58,59]. There are few long-term indoor measurements of FAPs that span several months [57].

The objective of this study is to integrate real-time measurements of FAP concentrations and size distributions (0.5–10 μm), human occupancy, and building ventilation conditions to evaluate the temporal dynamics of human-emitted fluorescent biological and abiotic particles in an open-plan office environment. A 3-month measurement campaign was conducted in one of the four Living Laboratory (LL) offices at the Purdue University Ray W. Herrick Laboratories [60,61]. The LL office includes a novel occupancy sensing array and an advanced building automation system that monitors and controls the HVAC system and a full-size double skin glass façade. This enabled implementation of both mechanical and natural ventilation modes during the campaign.

2. Materials and methods

2.1. Measurement of fluorescent aerosol particles via laser-induced fluorescence

FAP concentrations and size distributions were measured in the LL office via a LIF-based instrument – the Wideband Integrated Bioaerosol Sensor (WIBS) (WIBS-NEO, Droplet Measurement Technologies LLC, Longmont, CO, U.S.A.). The WIBS is a single particle fluorescence spectrometer that measures the optical equivalent diameter (D_o), fluorescence characteristics, and asymmetry factor (AF) of particles in real-time [62].

The WIBS uses a 635 nm continuous laser diode and two pulsed Xenon ultraviolet (UV) sources (at 280 nm and 370 nm) [63,64]. The particle stream is first directed towards the 635 nm laser diode using a laminar flow system. Here, elastic scattering intensity is measured for each particle at a 90° offset as they pass the laser diode [51]. This scattered intensity is used to determine D_o (WIBS D_o range: 0.5–30 μm) via Mie scattering theory [52]. WIBS optical size classification (D_o vs. physical diameter) was periodically evaluated throughout the campaign using polystyrene latex spheres; an example is shown in Fig. S1. Next, a quadrant photomultiplier tube probes the forward scattering intensity at four angular offsets to calculate the AF [51]. The AF is an approximate representation of particle shape, with AF = 0 to 15: spherical or nearly spherical particles; AF = 15 to 30: aspherical particles; and AF = 30 to 100: rod or fiber-shaped particles [47]. After the particle passes the laser diode, it is subjected to UV irradiation via two sequential UV pulses peaking at 280 nm and 370 nm [51,52]. The resulting particle fluorescence from each excitation is captured, filtered, and sent to two different fluorescence detectors: FL1 (detects light from 310 to 400 nm) and FL2 (detects light from 420 to 650 nm) [64].

The WIBS provides three fluorescence excitation and emission channels: Channel A (excitation: 280 nm, emissions: 310–400 nm), Channel B (excitation: 280 nm, emissions: 420–650 nm), and Channel C (excitation: 370 nm, emissions: 420–650 nm). The WIBS reports the emissions in each channel in terms of numerical values of arbitrary units. Thus, to ascertain if a particle has or has not exhibited fluorescence, threshold emission values are calculated for all three channels using the forced trigger method [47,51,52]. In forced trigger, the Xenon UV lamps are operated in the absence of sample flow to determine the background fluorescent emissions in each channel [47]. Particles are considered fluorescent in a channel if they exceed the mean background fluorescence intensity plus three times its standard deviation measured for that channel [13,47,62,65]. The forced trigger calculation was performed once per day during the measurement campaign.

A single particle can fluoresce in more than one channel. Therefore, fluorescent particles detected via the WIBS can be grouped into seven categories: (I) Type 'A' (exhibiting fluorescence only in Channel A), (II) Type 'B' (exhibiting fluorescence only in Channel B), (III) Type 'C' (exhibiting fluorescence only in Channel C), (IV) Type 'AB' (exhibiting fluorescence in both Channel A and Channel B), (V) Type 'BC' (exhibiting fluorescence in both Channel B and Channel C), (VI) Type 'AC' (exhibiting fluorescence in both Channel A and Channel C), and (VII) Type 'ABC' (exhibiting fluorescence in all the three channels).

The WIBS output file contains size-resolved single particle data at > 1 Hz time-resolution. In this study, particles from D_o = 0.5–10 μm were selected for analysis. A custom-written Python code converted single particle data into a time-series of size-resolved number concentrations of total particles (fluorescent and non-fluorescent) (N_T, m^{-3}) and fluorescent particles (N_F, m^{-3}) with a moving average over a 30 min window with a step size of 1 min. Number concentrations were grouped into nine bins of the following D_o widths: 0.5–0.65 μm, 0.65–0.8 μm, 0.8–1 μm, 1–2 μm, 2–3 μm, 3–4 μm, 4–5 μm, 5–7.5 μm, and 7.5–10 μm. The size-resolved number concentrations were converted to size-resolved volume concentrations assuming spherical particles [66] and then to size-resolved mass concentrations assuming a density of 1 g cm^{-3} [13,52]. Size-integrated particle mass concentrations (D_o = 0.5–10 μm) were calculated for both total (PM_T, μg m^{-3}) and fluorescent (PM_F, μg m^{-3}) particles. As the density for indoor particles from D_o = 0.5–10 μm can range from about 1 to 2.5 g cm^{-3} [5], the *PM* concentrations reported here can be considered as lower bounds of the true *PM* [13]. Size-resolved concentrations were converted to lognormal size distributions as: total particles, number: $dN_T/dlogD_o$ (m^{-3}); FAPs, number: $dN_F/dlogD_o$ (m^{-3}); total particles, mass: $dM_T/dlogD_o$ (μg m^{-3}); and FAPs, mass: $dM_F/dlogD_o$ (μg m^{-3}). FAP concentrations and size distributions were further partitioned among FAP types (A, B, C, AB, BC, AC, ABC). Size-resolved particle number concentration ratios (N_F/N_T) and size-integrated particle mass concentration ratios (PM_F/PM_T) were calculated to quantify the fractional amount of total particles that exhibited fluorescence.

As the WIBS is a single particle instrument, situations may arise where two particles pass through the irradiation channel simultaneously before the Xenon UV lamps recharge themselves. In such a case, the second particle is counted, but its fluorescence is not captured. These situations are typical in environments with high particle loadings, and are corrected using a dead time correction factor [50,58]. However, the particle concentrations in the studied environment were comparatively low (Fig. 1). For example, on the day with the highest observed particle number concentrations during the campaign, the error due to missed particles was approximately 4.9%. Thus, due to the low likelihood of missing particles, dead time corrections were not used.

2.2. Measurement of seated occupancy via a chair-based temperature sensor array

Seated occupancy in the LL office was measured with a chair-based temperature sensor array, as described in Wagner et al. (2021) [36]. The LL office includes twenty desk-chair pairs assigned to graduate students that are organized in a grid of four rows of five desks each (Fig. S2). Each chair was equipped with a K-type epoxy coated tip thermocouple (TC-PVC-K-24-180, Omega Engineering Inc., Norwalk, CT, U.S.A.) connected to a battery-powered datalogger (EasyLog EL-USB-TC, Lascar Electronics Inc., Erie, PA, U.S.A.). Total seated occupancy was calculated with a time-resolution of 15 s. In this study, the total seated occupancy is a proxy for total room occupancy as the

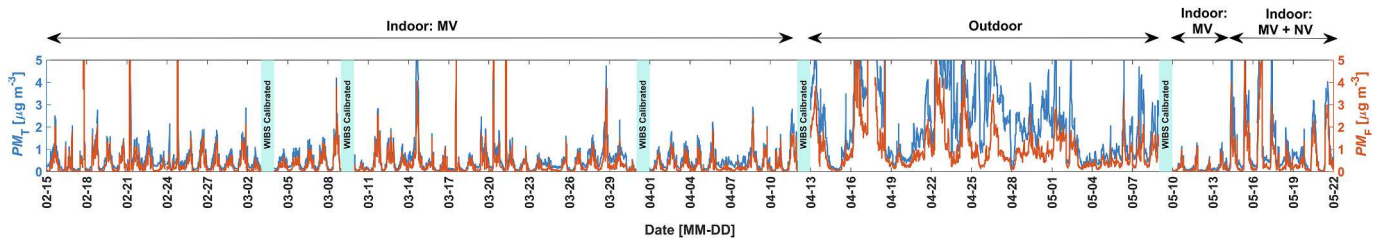

Fig. 1. Complete time-series of size-integrated total particle and FAP mass concentrations in indoor air (under MV and MV + NV modes) and outdoor air as measured by the WIBS during the measurement campaign.

occupants were observed to remain seated aside from brief periods of standing entry and exit and group discussions. Graduate students in the LL office did not follow any specific work schedules and worked flexible hours.

2.3. Site description: Herrick Living Laboratory offices at Purdue University

The WIBS measurement campaign was conducted from February 15 to May 22, 2019 in one of the four Herrick LL offices in West Lafayette, IN, U.S.A [36,67–69]. The LL offices are part of a high-performance building that was awarded a LEED Gold Certificate. The building was designed and constructed following criteria for future high-performance buildings and includes a state-of-the-art building automation and sensing platform and energy-efficient HVAC technologies. Each LL office has its own HVAC system that is monitored and controlled through a building automation system enabled by Tridium JACE controllers and the Niagara/AX software framework (Tridium Inc., Richmond, VA, U.S.A.) [67]. The LL office has hard tile flooring, painted walls, and ceiling tiles. The dimensions are 10.5 m × 9.9 m × 3.2 m (L × W × H) and the volume is 333 m^3.

The LL office operated under two ventilation modes during the WIBS measurement campaign: (1) mechanical ventilation (MV) and (2) mixed-mode ventilation with mechanical ventilation and natural ventilation (MV + NV). Under the MV mode, the LL office supply air contains a mixture of outdoor air and recirculated room air. After the outdoor air and recirculated room air are mixed, the MV supply air passes through an HVAC filter bank including a MERV 8 pre-filter with synthetic media and a MERV 14 filter with layered melt-blown synthetic media. NV is enabled by a south-facing, full-size double skin glass façade (Fig. S2). The fraction of outdoor air that enters via NV is not filtered. The MV supply and return air blowers are activated under the MV + NV mode to create a negative pressure in the LL office to entrain outdoor air through dampers located along the façade. The nominal supply air exchange rate under the two modes was 7 h^{-1} (same for day/night and weekday/weekend); this helped to ensure uniform mixing of indoor air in the LL office. The supply air exchange rate was determined using volumetric airflow rates obtained from the building automation system.

WIBS measurements during the campaign were conducted as follows: (1) indoor WIBS measurements under the MV mode from February 15 to April 11, 2019 and from May 10 to 13, 2019; (2) indoor WIBS measurements under the MV + NV mode from May 14 to 22, 2019; and (3) outdoor WIBS measurements from April 13 to May 08, 2019. During (1) and (2), the WIBS was housed in a custom-built sound enclosure with a vertical copper tube sample inlet (Fig. S2) to minimize sound propagation from the internal diaphragm pump and Xenon UV lamps. During (3), the WIBS sampled from the outdoor air duct of the HVAC system via an isokinetic probe.

3. Results and discussion

The following sub-sections present selected results from the WIBS measurement campaign. First, temporal dynamics of indoor FAPs measured in the LL office under the MV mode are discussed. Second, properties of FAP types as categorized by the WIBS (A, B, C, AB, BC, AC, ABC) for the LL office under the MV mode are presented. Third, characteristics of indoor FAPs in the LL office under the MV mode are compared to those measured outdoors and in the LL office under the MV + NV mode. Finally, the indoor FAP measurements are discussed within the broader context of indoor biological particle dynamics and microbiology.

3.1. Temporal dynamics of fluorescent aerosol particles in the LL office under mechanical ventilation

Fig. 1 presents the complete time-series of the size-integrated total (PM_T) and fluorescent (PM_F) particle mass concentrations as measured by the WIBS during the measurement campaign. For the LL office under the MV mode, PM_T ranged from 0.033 to 7.487 μg m^{-3} (mean PM_T = 0.62 μg m^{-3}), PM_F ranged from 0.004 to 6.762 μg m^{-3} (mean PM_F = 0.39 μg m^{-3}), and the mean size-integrated FAP number concentration was $N_F = 4.2 \times 10^4$ m^{-3}. Similar indoor FAP number concentrations were reported for occupied days in a classroom in California, U.S.A. (mean $N_F = 3.9 \times 10^4$ m^{-3}) [54] and during the summer months in a two-occupant residence in California, U.S.A. (mean $N_F = 4 \times 10^4$ m^{-3}) [57]. Comparable N_F have been measured in outdoor air during the summer months in Hyytiälä, Finland (mean $N_F = 4.6 \times 10^4$ m^{-3}) [49]. However, the mean N_F for the LL office was lower than that for a hospital in Brisbane, Australia (mean $N_F = 6 \times 10^4$ m^{-3}) [55].

Fig. 2 presents temporal trends in total and fluorescent particle number and mass concentrations and size distributions, human occupancy, and indoor environmental conditions for a one-week period during the measurement campaign (April 01 to 07, 2019). The LL office remained under the MV mode with a nominal supply air exchange rate of 7 h^{-1} and a mean recirculation ratio of 0.36. A distinct temporal trend is evident whereby the abundance of super-micron total and fluorescent particles followed human occupancy patterns. FAP number and mass concentrations for $D_o > 1$ μm were greater during occupied periods as compared to unoccupied periods and during weekdays as compared to weekends (Fig. 2). Coarse mode FAPs contributed significantly to total particle concentrations during occupied periods, with PM_F/PM_T scaling with occupancy. During occupied periods, PM_F/PM_T varied from 0.5 to 0.8 and N_F/N_T exceeded 0.7 for $D_o > 4$ μm. Diurnal profiles of PM_F/PM_T and occupancy were similar during weekdays (Fig. 3). Across all days under the MV mode, the mean PM_F/PM_T was 0.34 for 0 occupants, 0.56 for 1 to 3 occupants, 0.68 for 3 to 6 occupants, and 0.72 for >6 occupants. Collectively, these results demonstrate that humans are a major source of super-micron FAPs in mechanically ventilated office buildings. Prior chamber studies confirm that human emissions enrich the indoor atmosphere with FAPs [1,13,14,56,70].

PM_F/PM_T was more strongly associated with occupancy as compared to N_F/N_T (Figs. 3 and S3). As illustrated in Fig. 4, size-resolved N_F/N_T profiles were nearly identical for occupancy groupings of 1–3, 3 to 6, and >6. Thus, the size-resolved contribution of FAPs to total particle number concentrations remains approximately the same for occupancy ≥1. However, N_F/N_T is a strong function of particle size. N_F/N_T

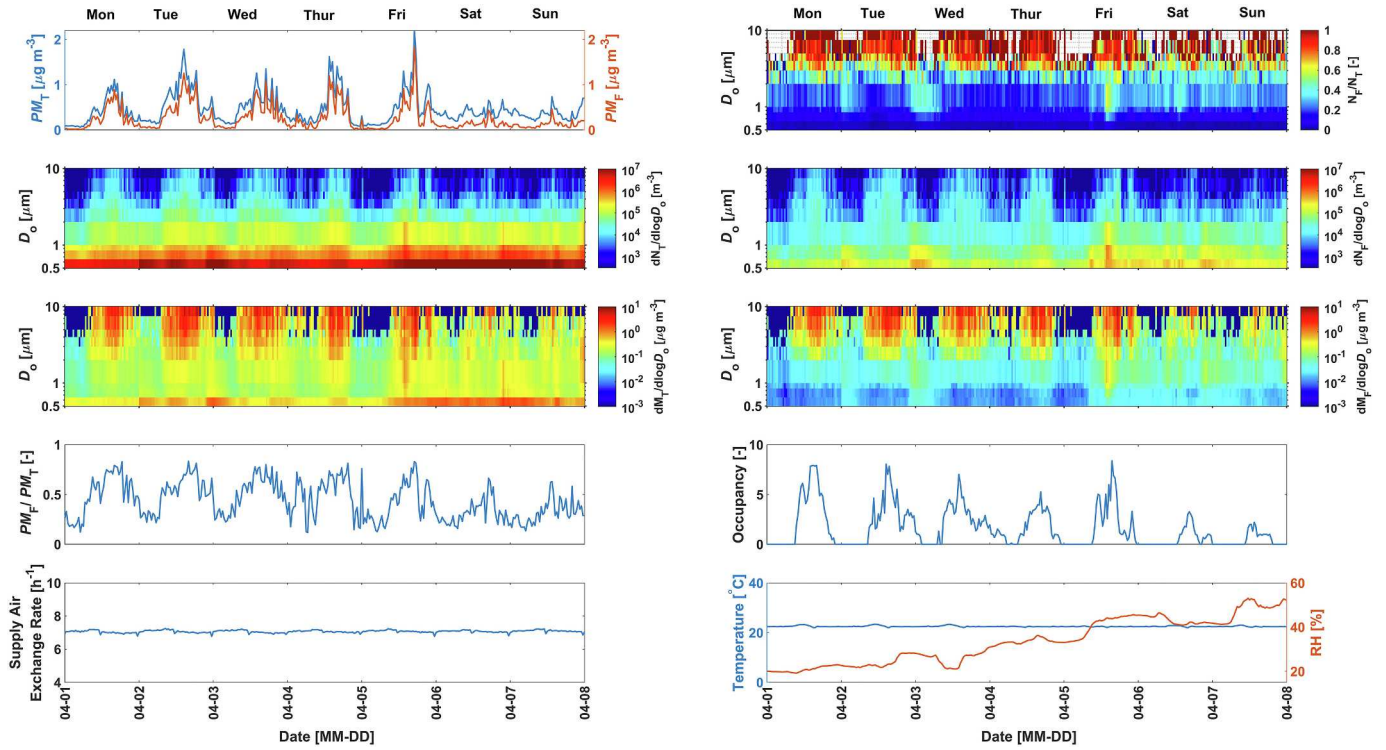

Fig. 2. Illustrative temporal sequence in the LL office for a one-week period (April 01 to 07, 2019) under the MV mode: (top-left) size-integrated total particle and FAP mass concentrations, (top-right) size-resolved ratios of FAP number concentrations to total particle number concentrations, (second-row-left) total particle number size distributions, (second-row-right) FAP number size distributions, (third-row-left) total particle mass size distributions, (third-row-right) FAP mass size distributions, (forth-row-left) ratios of size-integrated FAP mass concentrations to total particle mass concentrations, (forth-row-right) human occupancy, (bottom-left) supply air exchange rates, and (bottom-right) indoor air temperatures and relative humidities (RH).

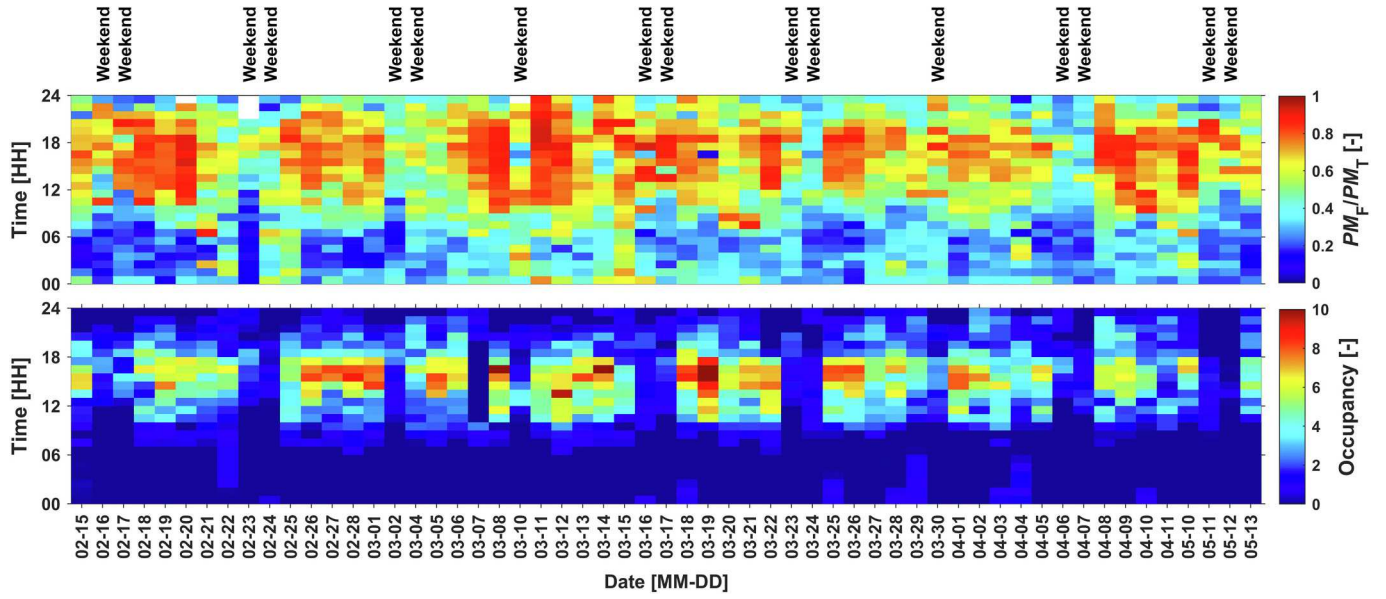

Fig. 3. Comparison of diurnal trends in the ratio of size-integrated FAP mass concentrations to total particle mass concentrations with human occupancy in the LL office for all days under the MV mode.

increased with particle size from D_o = 0.5–10 μm (Fig. 4). Across all occupied periods under the MV mode, the mean N_F/N_T was 0.10 for D_o = 0.5–1 μm, 0.33 for D_o = 1–3 μm, and 0.83 for D_o = 3–10 μm. Similar observations regarding the size-dependency of N_F/N_T in indoor environments were reported Li et al. (2020) [53] and Yang et al. (2021) [13]. Possible explanations include larger particles containing a greater number of fluorophores [65] and an increased prevalence of fluorescent biological and abiotic material among larger indoor particles [12]. Consequently, the number of FAPs were observed to exceed the number of non-FAPs from D_o = 3–10 μm across all occupancy regimes (Fig. S4). Nevertheless, both super-micron FAPs and non-FAPs scaled with occupancy. The size-resolved ratio of FAPs to non-FAPs (by number) did not change significantly with occupancy in the sub-micron region; however, it increased significantly during occupied periods in the super-micron

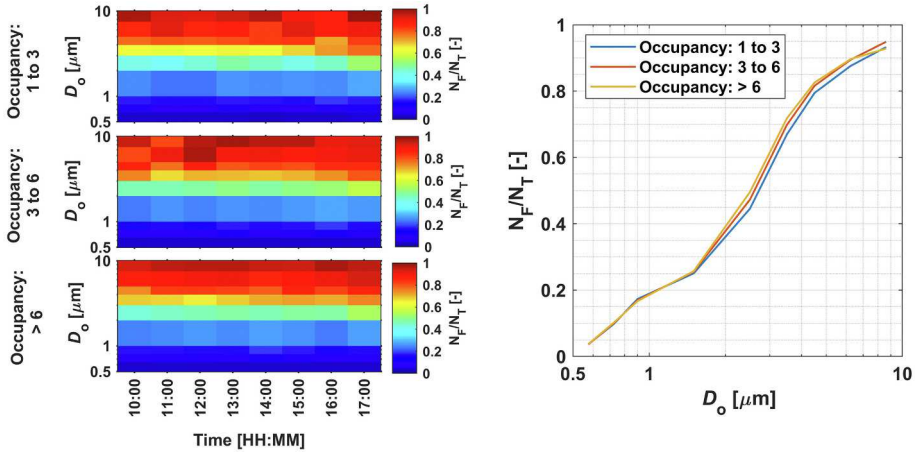

Fig. 4. Size-resolved ratios of FAP number concentrations to total particle number concentrations for different occupancy groupings in the LL office for all days under the MV mode: (left) mean size-resolved ratios per hour of the day and (right) mean size-resolved ratios for each occupancy grouping.

region (Fig. S4). This corroborates the earlier stated observation that humans are a major source of super-micron FAPs in mechanically ventilated office buildings. It should be noted that on some occasions, high PM_F/PM_T ratios were observed during low to zero occupancy periods (Fig. 3). This is likely due to the transport of FAPs of outdoor origin to the LL office via the supply air.

To further illustrate the temporality in FAP concentrations in the LL office under the MV mode, Fig. 5 presents two illustrative sequences involving human occupancy transitions over 24 h (**case I, top panel**) and a floor cleaning event (**case II, bottom panel**). For case 1, total and fluorescent particle mass concentrations (PM_T, PM_F) track occupancy as the LL office transitions from an occupied period (12:00 to 23:00) to an unoccupied period (23:00 to 07:00) and back to an occupied period (07:00 to 12:00). In the absence of humans during the unoccupied period, PM_F drops to below 0.1 μg m^{-3} and the office air is nearly devoid of FAPs with $D_o > 3$ μm. The sudden decrease in FAP concentrations for D_o = 3–10 μm as occupants leave the LL office can be attributed to accelerated FAP removal via gravitational settling to indoor surfaces, ventilation (exhaust to outdoors), and HVAC filtration [71,72]. FAPs from D_o = 0.5–3 μm, however, did not exhibit this rapid decay and were detected during the unoccupied period. The presence of fluorescent and non-fluorescent particles during this period are likely attributed to

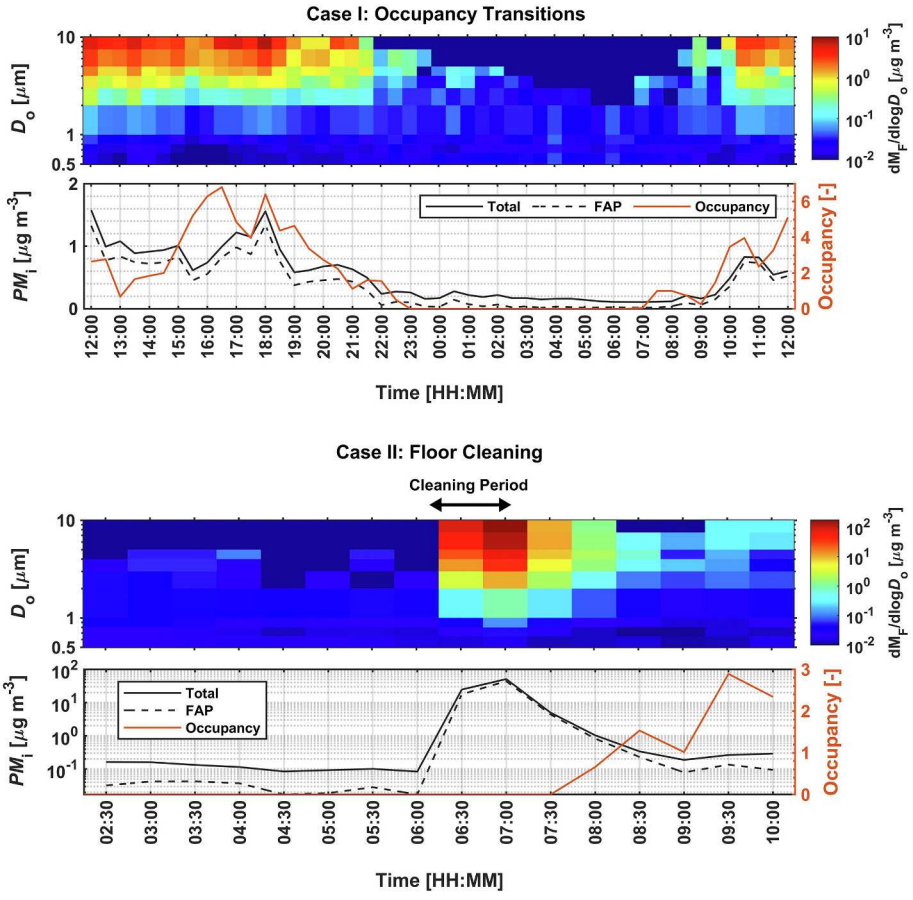

Fig. 5. Illustrative short-term temporal sequences in the LL office under the MV mode: (top) case I: human occupancy transitions over 24 h from February 19 to 20, 2019 and (bottom) case II: floor cleaning event (dry sweeping and wet mopping) on March 21, 2019. FAP mass size distributions, size-integrated total particle and FAP mass concentrations, and human occupancy are shown for each example case. Note: for case II, the seated occupancy was zero during the cleaning event, however, the LL office was occupied by one custodial staff member.

particle delivery to the LL office via the supply air given the reduced removal efficiency for particles from D_o = 0.5–3 μm by the MERV 8 pre-filter and for particles from D_o = 0.5–1 μm by the MERV 14 filter in the HVAC system [73]. As the supply air is a mixture of outdoor and recirculation air, the detected FAPs include outdoor FAPs and indoor FAPs released during occupied periods that remain airborne prior to removal via surface deposition, ventilation (exhaust to outdoors), and HVAC filtration.

Table S1 summarizes size-resolved particle deposition loss rate coefficients from D_o = 0.5–10 μm from selected studies. For the analyzed period, the LL office nominal supply air exchange rate was 7 h^{-1}. Thus, the deposition loss rate coefficients suggest that for particles from D_o = 0.5–3 μm, removal via ventilation is the dominant loss mechanism, whereas for particles from D_o = 3–10 μm, both removal via deposition (gravitational settling) and ventilation are relevant. Furthermore, the deposition loss rate coefficients indicate that particle deposition from D_o = 0.5–10 μm scales with particle size (also observed in Fig. 5).

Cleaning the hard flooring of the LL office by a custodial staff member was associated with a sudden increase in FAP mass concentrations (Fig. 5, case II, bottom panel). The cleaning period began at around 06:00, continued until 07:00, and occurred during a period of zero seated occupancy. Dry sweeping and wet mopping were sequentially conducted. Indoor FAPs increased nearly 2200-fold, from PM_F = 0.02 μg m^{-3} prior to floor cleaning to a maximum of PM_F = 44.12 μg m^{-3}. An equivalent increase was observed for total particles (PM_T). Following the cleaning event, FAPs decayed toward background concentrations over a period of 2 h. The majority of emitted FAPs were in the coarse mode, with D_o > 1 μm. This suggests that floor cleaning activities can be important episodic sources of super-micron FAPs in office environments [74]. The FAPs were likely released into the air via the resuspension of settled FAPs on the floor surface [21] during dry sweeping, and to a lesser extent, during wet mopping.

Throughout the WIBS measurements in the LL office under the MV mode, the air temperature (T) varied between 20 and 28 °C and the relative humidity (RH) varied between 10 and 60%. Prior research suggests that RH can influence FAP emissions from the human envelope [13,75]. To discern the role of T and RH on the relative abundance of FAPs in the LL office, PM_F/PM_T was plotted against T and RH (Fig. S5) for three occupancy groupings. It is evident that T and RH have no meaningful impact on PM_F/PM_T (R^2 < 0.05). Thus, under the range of indoor environmental conditions measured, T and RH do not influence the relative abundance of indoor FAPs.

3.2. Fluorescent aerosol particle apportionment in the LL office under mechanical ventilation

The multi-channel single particle fluorescence data provided by the WIBS enables classification of indoor FAPs among seven categories: A, B, C, AB, BC, AC, and ABC. Such categorization provides a basis for elucidating the possible biological and abiotic origins of the FAPs in the LL office (discussed later in **Section 3.4**). Fig. 6 presents the apportionment of the size-integrated FAP mass concentrations and FAP mass size distributions by FAP type over a one-week period (April 01 to 07, 2019). Non-fluorescent particles are included in the former. ABC-type particles dominated size-integrated FAP mass concentrations and contributed significantly to FAP mass size distributions for D_o > 2 μm. ABC-type and non-fluorescent particles were similar in magnitude during occupied periods. Mass concentrations and size distributions of ABC-, A-, and AB-type particles closely followed occupancy patterns in the LL office. On some days, so did B-type particles. A-, B-, and C-type particles contributed meaningfully to sub-1 μm mass size distributions during both occupied and unoccupied periods. AC-type particles were seldom detected.

The relative contribution of each FAP type to FAP mass and number concentrations for all days under the MV mode are provided in Table 1. ABC-type particles contributed >50% to indoor FAP mass, while A-, B-, and AB-type particles contributed 10–11%. FAP number concentrations were dominated by A-, B-, and C-type particles. These results are consistent with those reported by Yang et al. (2021) [13] and Zhou et al. (2017) [75].

The size-resolved apportionment of each FAP type on a number-basis is presented in Fig. 7 (right panel) (number size distributions resolved by FAP type are provided in Fig. S6). Sub-micron FAPs are dominated by A-, B-, and C-type particles. Together, they contribute more than 90% to the

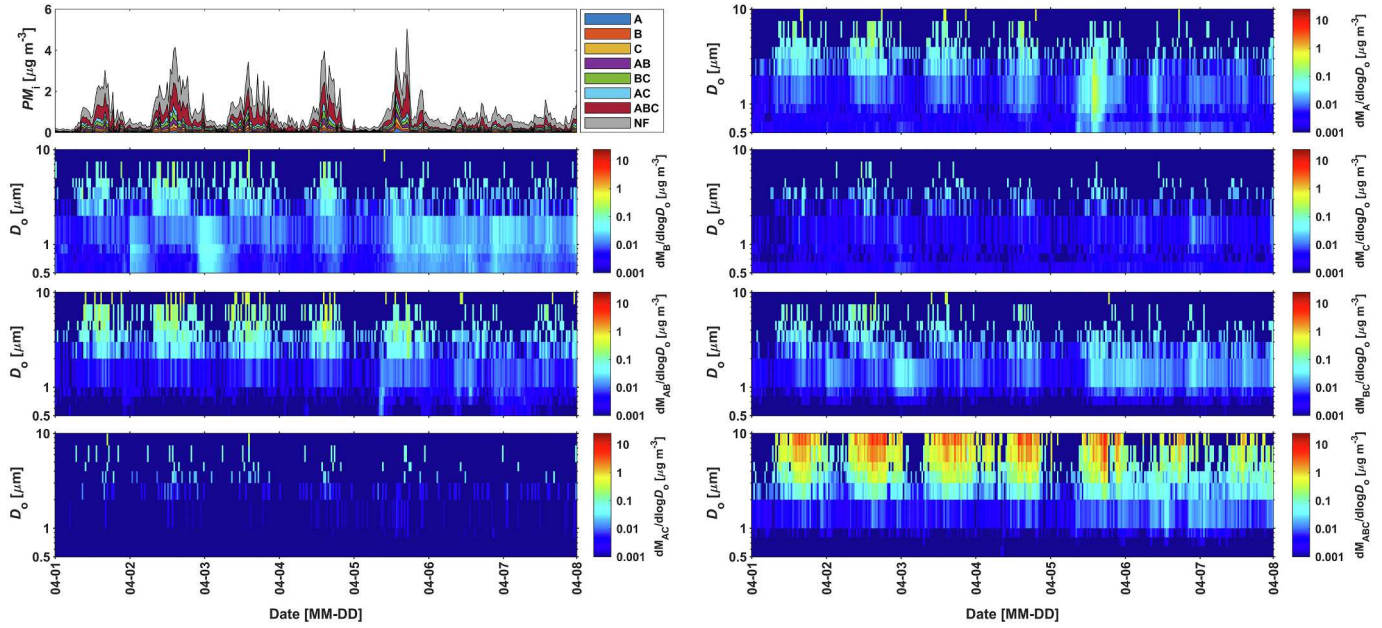

Fig. 6. Illustrative temporal sequence of FAP apportionment in the LL office for a one-week period (April 01 to 07, 2019) under the MV mode: (top-left) stacked size-integrated particle mass concentrations partitioned by FAP type (A, B, C, AB, BC, AC, and ABC) and non-fluorescent (NF) particles (an enlarged version is shown in Fig. S7 for better readability), (top-right) A-type mass size distributions, (second-row-left) B-type mass size distributions, (second-row-right) C-type mass size distributions, (third-row-left) AB-type mass size distributions, (third-row-right) BC-type mass size distributions, (bottom-left) AC-type mass size distributions, and (bottom-right) ABC-type mass size distributions.

Table 1
Relative contribution of FAP types to indoor FAP number and mass concentrations in the LL office for all days under the MV mode. Values listed as: mean (standard deviation).

FAP Type	Contribution to FAP Number (N_F)	Contribution to FAP Mass (PM_F)
A	30.21% (11.75%)	10.68% (10.78%)
B	30.29% (10.30%)	10.39% (9.47%)
C	13.33% (4.63%)	3.52% (4.64%)
AB	8.04% (3.09%)	10.99% (8.26%)
BC	6.69% (3.41%)	6.73% (7.72%)
AC	0.61% (0.42%)	0.91% (3.06%)
ABC	10.83% (8.29%)	56.80% (25.44%)

smallest WIBS size fraction measured, $D_o = 0.5–0.65$ μm. Conversely, A-, B-, and C-type particles contribute negligibly to size fractions with $D_o >$ 3 μm. Thus, while A-, B-, and C-type particles dominate the number of indoor FAPs, their comparatively small size limits their contribution towards FAP mass concentrations (Fig. 6). For ABC-type particles, approximately 58% are found in the $D_o = 1–4$ μm size fraction and 28% in the $D_o = 4–10$ μm size fraction. Although ABC-type particles are low in number (Table 1), their contribution to coarse mode FAPs is large, thus, they dominate FAP mass concentrations in the LL office (Fig. 6). AB-type particles exhibited a mode at $D_o = 2–3$ μm. As a result, they contributed second most to FAP mass. BC- and AC-type particles contributed to all size fractions, the latter at very small percentages.

Temporal variations in the apportionment of each FAP type on a number-basis is presented in Fig. 7 (left panel) for a one-week period (April 01 to 07, 2019). As occupancy increases on weekdays (April 01 to 05, 2019), so does the proportion of A- and ABC-type particles. The contribution of C-, AB-, and BC-type particles to FAP number concentrations did not show a strong association with occupancy during this week. Correlation coefficients of human occupancy with apportionment of each FAP type (by number) in the LL office under the MV mode were: 0.33 for A-type particles, −0.53 for B-type particles, −0.18 for C-type particles, −0.08 for AB-type particles, −0.08 for BC-type particles, 0.23 for AC-type particles, and 0.64 for ABC-type particles. This suggests that the office occupants were strong emitters, by number, of ABC-type particles, and to a lesser extent, A-type particles. Conversely, B-type particles (by number) exhibited a significant negative correlation with occupancy. Their relative abundance increased as the occupancy was reduced during the night hours and weekends (Fig. 7). This suggests that B-type particles (by number) are likely of outdoor origin, introduced to the LL office via the HVAC system.

Diurnal trends in the ratio of the number of each FAP type to the total number of FAPs (e.g. N_A/N_F) are shown in Fig. 8 for all days under the MV mode. Variability in the relative number of each FAP type was observed over the duration of the measurement campaign. For example, on some weekdays, N_A/N_F often exceeded 0.5 (e.g. February 26 to March 01, 2019), while on most others N_A/N_F generally remained below 0.4. The ratio of ABC-type particles to total FAPs on a number-basis often tracked occupancy patterns in the LL office during the campaign. The floor cleaning periods in the morning hours on February 21, March 20, and March 21, 2019 were enriched with ABC-type particles ($N_{ABC}/N_F >$ 0.4 on February 21 and March 21, 2019). The number contribution of AB-type particles also rose during these periods. Thus, floor cleaning (sweeping and mopping) is a source of ABC- and AB-type particles. Ratios of B- and C-type particles showed no distinguishable diurnal trends.

Collectively, the results presented in Figs. 6–8 demonstrate that human occupants are a major source of ABC-type particles (number and mass), and to a lesser extent, A-type particles (number and mass), AB-type particles (mass only), and B-type particles (mass only). Human occupants were not a major contributor to C-, BC-, and AC-type particles (number and mass). During the unoccupied periods, FAPs were generally dominated by A-, B-, and C-type particles (by number). Thus, they were very likely supplied to the LL office via the supply air. As all three FAP types were most associated with sub-micron particles, they had the highest likelihood of penetrating through the MERV 8 and 14 filters in the HVAC system, thereby entering the LL office with the supply air.

Probability distribution functions of the asymmetry factor (AF, proxy for particle shape) for each FAP type under two occupancy groupings (low: < 3 occupants and high: > 3 occupants) for all days under the MV mode are presented in Fig. 9. The AFs for each FAP type followed lognormal distributions, as suggested by Xie et al. (2017) [58]. The AF modes of A-, B-, C-, AB-, BC-, and AC-type particles lie within the range of AF = 1 to 10, indicating that these particles are predominantly spherical or nearly spherical [47]. In addition, their AF distributions remain unchanged during periods of low and high occupancy in the LL office. ABC-type particles, however, exhibit different trends in AF distributions. During low occupancy periods, the AF distribution of ABC-type particles is like that of other FAP types, implying a largely spherical or nearly spherical form. However, as the occupancy increases, the frequency of ABC-type particles with AF > 10 rises (AF distribution

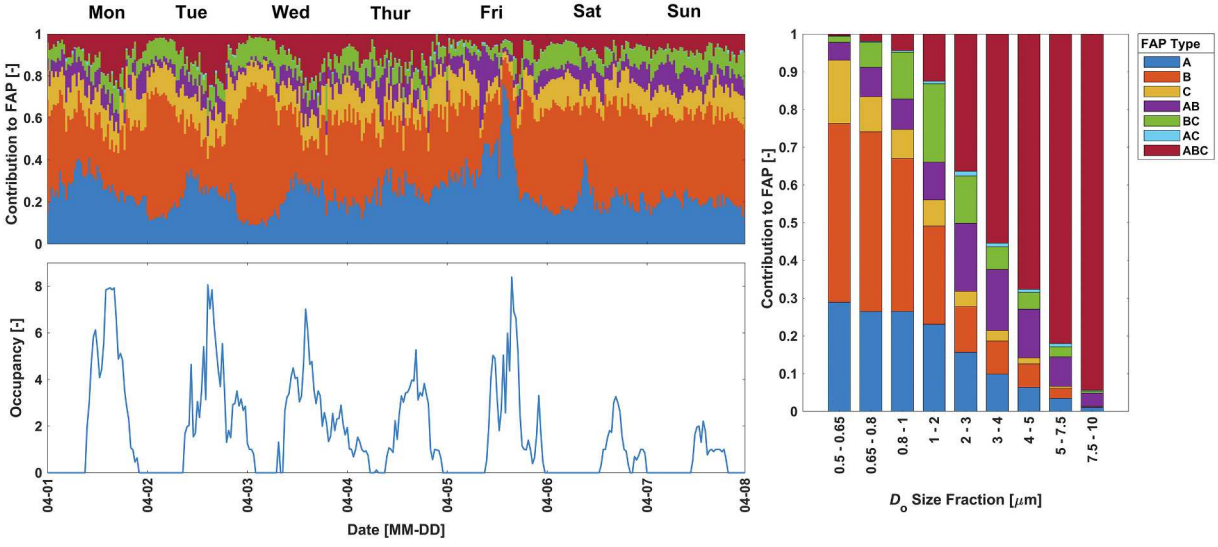

Fig. 7. FAP apportionment in the LL office for a one-week period (April 01 to 07, 2019) under the MV mode: (left) comparison of the time-resolved relative contribution of FAP types to FAP number concentrations with human occupancy and (right) mean size-resolved relative contribution of FAP types to FAP number concentrations.

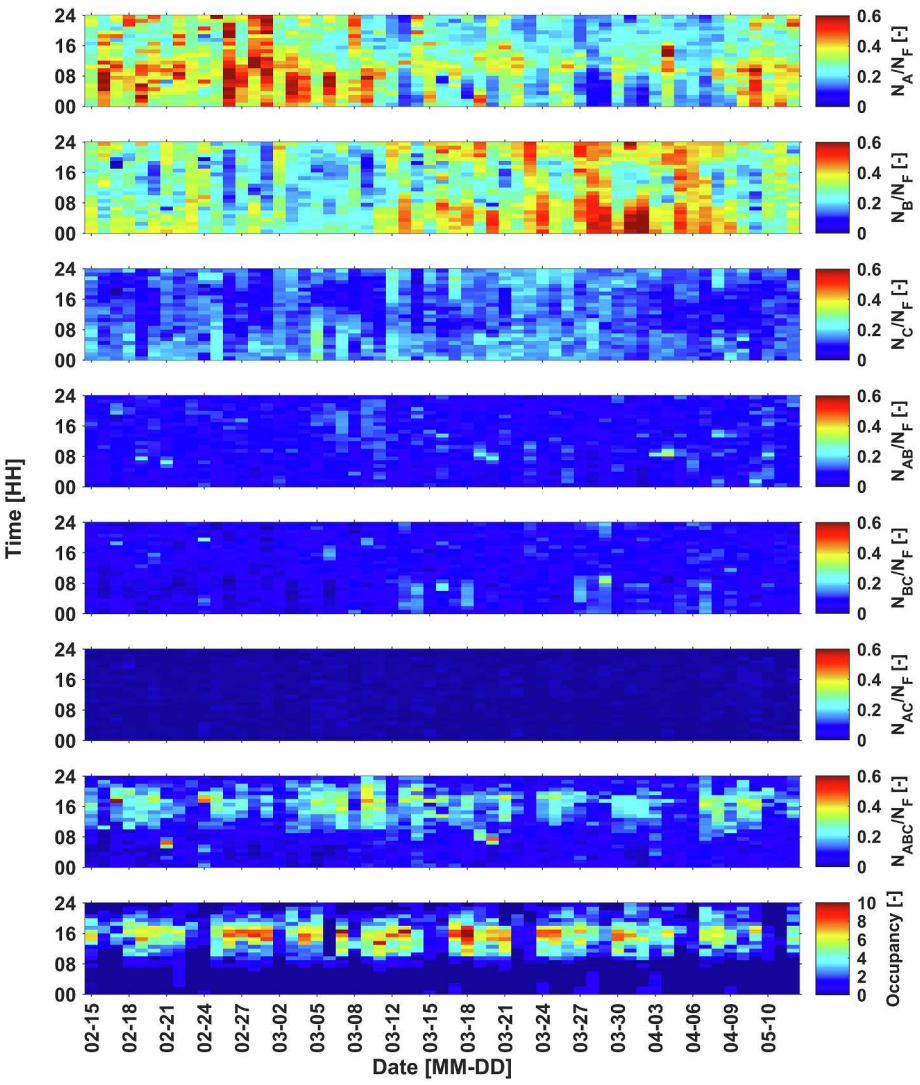

Fig. 8. Comparison of diurnal trends in the ratio of the number concentrations for each FAP type to total FAP number concentrations with human occupancy in the LL office for all days under the MV mode: (first row) A-type number ratios, (second row) B-type number ratios, (third row) C-type number ratios, (fourth row) AB-type number ratios, (fifth row) BC-type number ratios, (sixth row) AC-type number ratios, (seventh row) ABC-type number ratios, and (eighth row) human occupancy.

becomes bimodal with one mode at AF < 1 and another mode at AF $>$ 10). This suggests that ABC-type particles associated with human emissions in the LL office likely include variable morphologies (spherical, aspherical, and fiber-like).

3.3. Fluorescent aerosol particles: outdoors vs. indoors under mechanical and natural ventilation

Indoor FAP mass and number concentrations in the LL office varied between the MV and MV + NV modes, with higher concentrations observed under the latter (Figs. 1 and 10 and Table 2). This is consistent with the elevated levels of outdoor FAPs on both a mass- and number-basis. The mean PM_F for outdoor air was 2.82-fold greater than that indoors under the MV mode. The MV + NV mode increased the mean indoor PM_F by a factor of 1.92 compared to the MV mode. Mean FAP number concentrations increased from $N_F = 4.2 \times 10^4$ m^{-3} under the MV mode to $N_F = 6.1 \times 10^4$ m^{-3} under the MV + NV mode. Under the MV + NV mode, unfiltered outdoor air enters the LL office via dampers located along the double skin façade (mean outdoor air exchange rate of 2.55 h^{-1}). This offers efficient entry of outdoor FAPs of biological and abiotic origin across all size fractions into the office environment [76]. A recent study also observed an increase in concentrations of total particles in an office when natural ventilation was introduced [77]. Under the MV mode, some fraction of outdoor FAPs is removed via the HVAC filters [78]. Thus, the filters act to protect the LL office from outdoor FAPs, while enhancing the relative contribution of indoor-generated and human-associated FAPs during occupied periods.

Diurnal and weekly trends in size-integrated FAP mass concentrations partitioned by FAP type for indoor air under both ventilation modes and outdoor air are shown in Fig. 10. Non-fluorescent particles are also included. In general, the apportionment of FAPs by FAP type was similar between outdoor air and indoor air under both ventilation modes (Table 2). The diurnal trend in PM_F/PM_T more closely followed occupancy patterns under the MV mode as compared to the MV + NV mode. FAP profiles under the MV + NV mode are influenced by both occupancy and the significant outdoor-to-indoor transport of FAPs across the double skin façade. The latter perturbs the strong FAP-occupancy association for PM_F/PM_T observed under the MV mode. There were no discernible trends in the diurnal pattern of PM_F/PM_T for outdoor air, however FAP mass concentrations were generally the greatest during the early morning and lowest during the night.

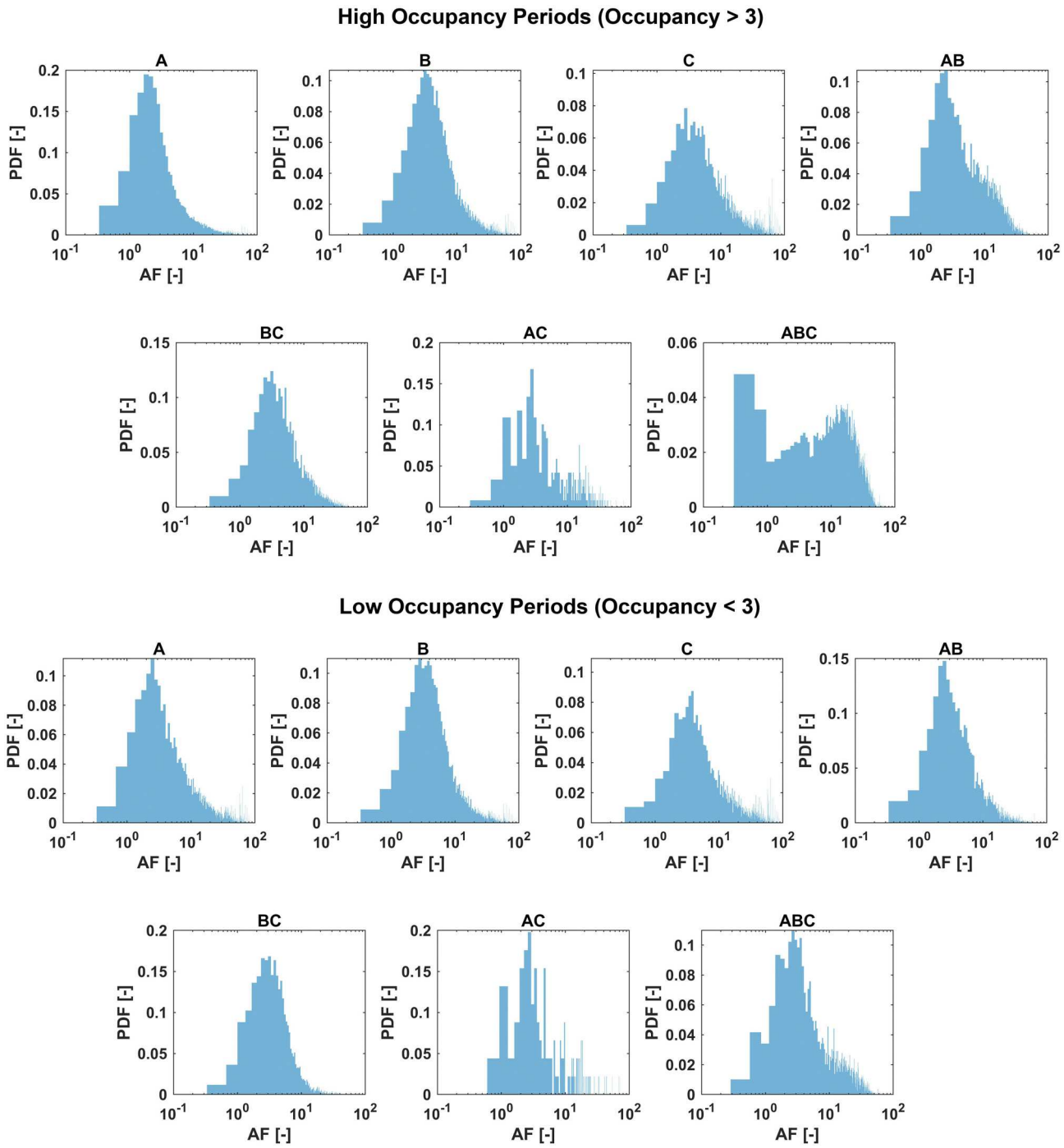

Fig. 9. Asymmetry factor (AF) probability distribution functions (PDFs) for each FAP type (A, B, C, AB, BC, AC, and ABC) resolved by occupancy in the LL office for all days under the MV mode.

3.4. Relating indoor fluorescent aerosol particles to biological particles: A qualitative discussion

The WIBS measurements in the LL office during occupied periods under the MV mode demonstrate that humans are a major source of super-micron FAPs, including ABC-, A-, B-, and AB-types (Figs. 2 and 6). Therefore, the majority of the measured FAPs with $D_o > 3$ μm during these periods are expected to be associated with human emissions. Human-associated emissions include FAPs released from the human envelope (skin, hair, clothing, exhaled breath) and human movement-induced FAP resuspension from indoor surfaces. As the LL office occupants remained seated aside from brief periods of standing entry and exit and group discussions, walking-induced FAP resuspension from the hard flooring was likely small compared to FAP emissions from the seated human envelope [12]. Similarly, FAP emissions from exhaled breath are expected to be small compared to FAP emissions from skin, hair, and clothing. Occupants were asked to keep speech to a minimum in the LL office and respiratory aerosol emissions for sedentary breathing are generally low [79,80].

The detected FAPs include a combination of biological and abiotic particles exhibiting fluorescence in the given excitation-emission bands of the WIBS [13,65]. Coarse mode FAPs released from the seated human envelope likely include bacterial and fungal aerosols, skin cells and fragments, and fluorescent clothing fabric fibers [13,81]. Human skin,

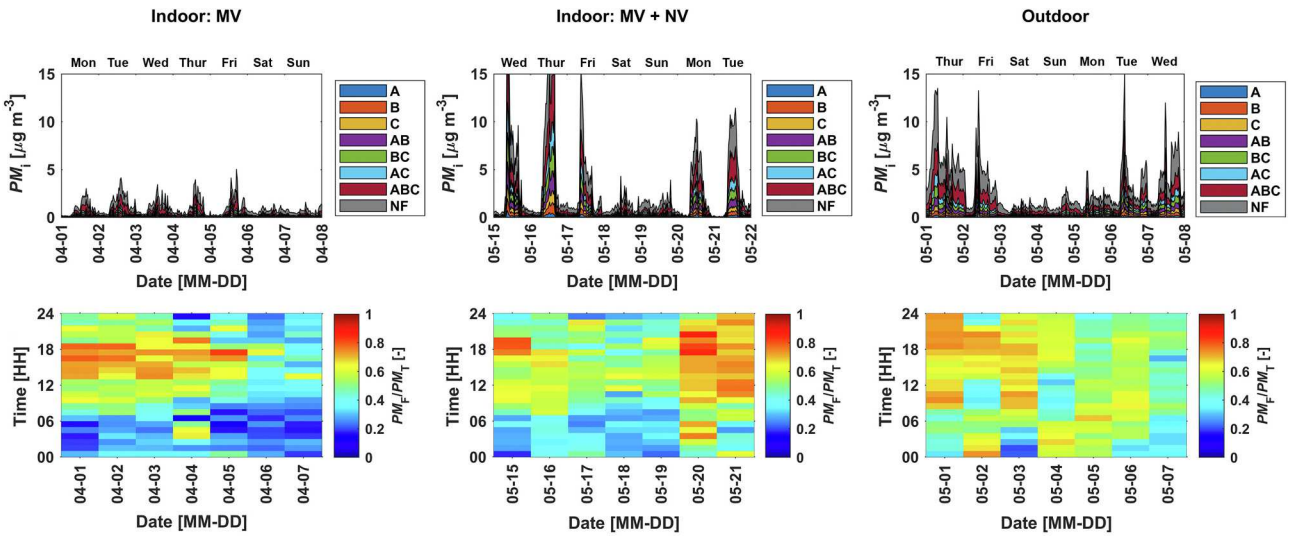

Fig. 10. Illustrative temporal sequences for: (left) LL office under MV mode (April 01 to 07, 2019), (middle) LL office under MV + NV mode (May 15 to 21, 2019), and (right) outdoor air (May 01 to 07, 2019). For each condition, the following are shown: stacked size-integrated particle mass concentrations partitioned by FAP type (A, B, C, AB, BC, AC, and ABC) and non-fluorescent (NF) particles (enlarged versions are shown in Fig. S8 for better readability) and ratios of size-integrated FAP mass concentrations to total particle mass concentrations.

Table 2
Summary of total particle and FAP number and mass concentrations in indoor air (under MV and MV + NV modes) and outdoor air. The relative contribution of FAP types to FAP number concentrations is provided. Values listed as: mean (standard deviation) across all days for each condition.

Parameter	Indoor Air: MV Mode	Indoor Air: MV + NV Mode	Outdoor Air
N_T	4.7×10^5 m^{-3} (3.8×10^5 m^{-3})	6.0×10^5 m^{-3} (4.8×10^5 m^{-3})	1.3×10^6 m^{-3} (2.0×10^6 m^{-3})
N_F	4.2×10^4 m^{-3} (8.4×10^4 m^{-3})	6.1×10^4 m^{-3} (5.0×10^4 m^{-3})	7.7×10^4 m^{-3} (5.7×10^4 m^{-3})
PM_T	0.62 μg m^{-3} (2.23 μg m^{-3})	1.35 μg m^{-3} (1.78 μg m^{-3})	2.17 μg m^{-3} (2.03 μg m^{-3})
PM_F	0.39 μg m^{-3} (1.53 μg m^{-3})	0.75 μg m^{-3} (1.47 μg m^{-3})	1.10 μg m^{-3} (1.04 μg m^{-3})
FAP Type	Contribution to FAP Number (N_F)		
A	30.21% (11.75%)	29.66% (10.14%)	32.26% (14.12%)
B	30.29% (10.30%)	27.10% (9.71%)	26.35% (7.79%)
C	13.33% (4.63%)	11.20% (6.08%)	9.48% (3.34%)
AB	8.04% (3.09%)	10.36% (3.68%)	11.20% (3.40%)
BC	6.69% (3.41%)	6.34% (2.78%)	6.81% (3.39%)
AC	0.61% (0.42%)	0.85% (0.59%)	0.83% (0.45%)
ABC	10.83% (8.29%)	14.49% (7.77%)	13.07% (5.34%)

hair, and oral/nasal cavities harbor a diversity of bacterial and fungal communities that can be shed into the indoor environment (along with skin cells), thereby shaping the office microbiome [40,82–84]. Clothing fabric fibers can be released into the air via textile friction induced by bodily movements [85].

The WIBS has been shown to reliably detect common bacterial and fungal aerosols of indoor origin [86], including bacterial groups such as *Mycobacterium*, *Pseudomonas*, *Acinetobacter*, *Micrococcus*, and *Staphylococcus* [2,15,30,34,35] and fungal groups such as *Aspergillus*, *Cladosporium*, *Fusarium*, *Penicillium*, *Phoma*, *Stachybotrys*, and *Ulocladium* [2,15,34]. Hernandez et al. (2016) [86] found most single bacterial cells to be categized as sub-micron A-type particles by the WIBS. However, single bacterial cells may be more commonly emitted from the human envelope in the form of larger bacterial cell agglomerates with D_o ~2–5 μm [12,34]. Thus, the increase in the number and mass of A-type particles during occupied periods in the LL office (Figs. 6–7) might be due to the emissions of bacterial cells and their agglomerates from the human envelope. Hernandez et al. (2016) [86] found the majority of the evaluated fungal aerosols to be classified as A- and AB-type particles, with a smaller fraction classified as B-, C-, AB-, AC-, and ABC-type particles. Such a broad fluorescence profile makes it difficult to relate the presence of fungal aerosols to specific FAP types measured in the LL office.

Clothing fabric fibers that are white in color or contain whitening agents associated with detergent residue [3,87] have been categorized as ABC-type particles and are typically associated with $D_o > 1$ μm [13,65]. It is likely a fraction of the detected coarse mode ABC-type particles during occupied periods are clothing fibers (Fig. S6). Such particles may have aspherical and fiber-like shapes. This may explain the increased prevalence of ABC-type particles with AF > 10 under high occupancy periods (Fig. 9). Clothing can also serve as a vector for the redistribution of environmental bacteria and fungi that deposit on clothing while in outdoor environments. One study found that clothed occupants are secondary emitters of bacteria and fungi of outdoor origin [14]. It is therefore likely that the observed human emissions of FAPs in the LL office include some contribution of secondary emissions of environmental bacterial and fungal aerosols from clothing.

Relating indoor FAPs to specific biological and abiotic particles is challenging without supplemental data, such as offline particle characterization with culture-, DNA-, and microscopy-based methods. While the WIBS enables real-time detection of FAPs, it lacks specificity and the size-dependency of particle fluorescence makes FAP identification based on a single threshold value challenging [65]. A recent literature review has outlined the major limitations of LIF-based instruments for real-time detection of biological FAPs [44]. Novel data-driven techniques can improve the ability of the WIBS to broadly identify FAP origins. For example, clustering analysis has been used to group measured FAPs into biological and abiotic categories [88–91]. Application of such techniques to evaluation of indoor FAP dynamics can provide additional insights on their possible origins.

4. Conclusion

Real-time measurements of fluorescent aerosol particles (FAPs), occupancy, and HVAC system operation were integrated together to

evaluate how humans and building ventilation conditions influence the indoor abundance of fluorescent biological and abiotic particles in an open-plan office environment. Indoor measurements with a laser-induced fluorescence (LIF)-based instrument (WIBS) in a living laboratory office demonstrated that humans are a major source of super-micron FAPs. Under mechanical ventilation, mass concentrations and size distributions of FAPs larger than 3 μm scaled with human occupancy in the office. Human occupants enriched the office with super-micron FAPs across a variety of fluorescence types (ABC-, A-, B-, and AB-types), some of which were associated with asymmetry factors suggestive of aspherical and fiber-like particle shapes. During unoccupied periods in the office under mechanical ventilation, FAPs larger than 3 μm were seldom detected. The introduction of unfiltered supply air via natural ventilation with a full-size double skin glass façade increased indoor FAP concentrations due to the efficient transport of outdoor FAPs to the office space. The measurements demonstrate how the composition of indoor air can change over variable time-scales due to time-dependent changes in human occupancy patterns and HVAC operational modes. While LIF offers valuable insights into the temporal dynamics of fluorescent biological and abiotic particles in a dynamically changing indoor environment, it has limitations that prevent unambiguous identification of particle types. Coupled online and offline measurement techniques can improve detection of specific biological and abiotic particles in occupied offices.

Declaration of competing interest

The authors declare that they have no known competing financial interests or personal relationships that could have appeared to influence the work reported in this paper.

Acknowledgements

Financial support was provided by the National Science Foundation (CBET-1805804). The authors would like to thank the staff at the Ray W. Herrick Laboratories for facilitating the work for this project.

Appendix A. Supplementary material

Supplementary material to this article can be found online at https://doi.org/10.1016/j.buildenv.2021.108249.

References

[1] S. Bhangar, R.I. Adams, W. Pasut, J.A. Huffman, E.A. Arens, J.W. Taylor, T. D. Bruns, W.W. Nazaroff, Chamber bioaerosol study: human emissions of size-resolved fluorescent biological aerosol particles, Indoor Air 26 (2016) 193–206, https://doi.org/10.1111/ina.12195.

[2] J.F. Meadow, A.E. Altrichter, S.W. Kembel, J. Kline, G. Mhuireach, M. Moriyama, D. Northcutt, T.K. O'Connor, A.M. Womack, G.Z. Brown, J.L. Green, B.J. M. Bohannan, Indoor airborne bacterial communities are influenced by ventilation, occupancy, and outdoor air source, Indoor Air 24 (2014) 41–48, https://doi.org/10.1111/ina.12047.

[3] D. Licina, W.W. Nazaroff, Clothing as a transport vector for airborne particles: chamber study, Indoor Air 28 (2018) 404–414, https://doi.org/10.1111/ina.12452.

[4] J. Qian, A.R. Ferro, Resuspension of dust particles in a chamber and associated environmental factors, Aerosol Sci. Technol. 42 (2008) 566–578, https://doi.org/10.1080/02786820802220274.

[5] A.R. Ferro, R.J. Kopperud, L.M. Hildemann, Source strengths for indoor human activities that resuspend particulate matter, Environ. Sci. Technol. 38 (2004) 1759–1764, https://doi.org/10.1021/es0263893.

[6] T. Wu, M. Fu, M. Valkonen, M. Täubel, Y. Xu, B.E. Boor, Particle resuspension dynamics in the infant near-floor microenvironment, Environ. Sci. Technol. 55 (2021) 1864–1875, https://doi.org/10.1021/acs.est.0c06157.

[7] S.R. Haines, R.I. Adams, B.E. Boor, T.A. Bruton, J. Downey, A.R. Ferro, E. Gall, B. J. Green, B. Hegarty, E. Horner, D.E. Jacobs, P. Lemieux, P.K. Misztal, G. Morrison, M. Perzanowski, T. Reponen, R.E. Rush, T. Virgo, C. Alkhayri, A. Bope, S. Cochran, J. Cox, A. Donohue, A.A. May, N. Nastasi, M. Nishioka, N. Renninger, Y. Tian, C. Uebel-Niemeier, D. Wilkinson, T. Wu, J. Zambrana, K.C. Dannemiller, Ten questions concerning the implications of carpet on indoor chemistry and microbiology, Build. Environ. 170 (2020) 106589, https://doi.org/10.1016/j.buildenv.2019.106589.

[8] B.E. Boor, M.P. Spilak, R.L. Corsi, A. Novoselac, Characterizing particle resuspension from mattresses: chamber study, Indoor Air 25 (2015) 441–456, https://doi.org/10.1111/ina.12148.

[9] B.E. Boor, J.A. Siegel, A. Novoselac, Monolayer and multilayer particle deposits on hard surfaces: literature review and implications for particle resuspension in the indoor environment, Aerosol Sci. Technol. 47 (2013) 831–847, https://doi.org/10.1080/02786826.2013.794928.

[10] M.P. Spilak, B.E. Boor, A. Novoselac, R.L. Corsi, Impact of bedding arrangements, pillows, and blankets on particle resuspension in the sleep microenvironment, Build. Environ. 81 (2014) 60–68, https://doi.org/10.1016/j.buildenv.2014.06.010.

[11] H.K. Hyytiäinen, B. Jayaprakash, P. V Kirjavainen, S.E. Saari, R. Holopainen, J. Keskinen, K. Hämeri, A. Hyvärinen, B.E. Boor, M. Täubel, Crawling-induced floor dust resuspension affects the microbiota of the infant breathing zone, Microbiome 6 (2018) 25, https://doi.org/10.1186/s40168-018-0405-8.

[12] T. Wu, M. Täubel, R. Holopainen, A.-K. Viitanen, S. Vainiotalo, T. Tuomi, J. Keskinen, A. Hyvärinen, K. Hämeri, S.E. Saari, B.E. Boor, Infant and adult inhalation exposure to resuspended biological particulate matter, Environ. Sci. Technol. 52 (2018) 237–247, https://doi.org/10.1021/acs.est.7b04183.

[13] S. Yang, G. Bekö, P. Wargocki, J. Williams, D. Licina, Human emissions of size-resolved fluorescent aerosol particles: influence of personal and environmental factors, Environ. Sci. Technol. 55 (2021) 509–518, https://doi.org/10.1021/acs.est.0c06304.

[14] R.I. Adams, S. Bhangar, W. Pasut, E.A. Arens, J.W. Taylor, S.E. Lindow, W. W. Nazaroff, T.D. Bruns, Chamber bioaerosol study: outdoor air and human occupants as sources of indoor airborne microbes, PloS One 10 (2015), e0128022, https://doi.org/10.1371/journal.pone.0128022.

[15] R.I. Adams, A.C. Bateman, H.M. Bik, J.F. Meadow, Microbiota of the indoor environment: a meta-analysis, Microbiome 3 (2015) 49, https://doi.org/10.1186/s40168-015-0108-3.

[16] M. Alsved, L. Bourouiba, C. Duchaine, J. Löndahl, L.C. Marr, S.T. Parker, A. J. Prussin, R.J. Thomas, Natural sources and experimental generation of bioaerosols: challenges and perspectives, Aerosol Sci. Technol. 54 (2020) 547–571, https://doi.org/10.1080/02786826.2019.1682509.

[17] S.K. Kerk, H.Y. Lai, S.K. Sze, K.W. Ng, A. Schmidtchen, S.S. Adav, Bacteria display differential growth and adhesion characteristics on human hair shafts, Front. Microbiol. 9 (2018) 2145, https://doi.org/10.3389/fmicb.2018.02145.

[18] D.A. Edwards, J.C. Man, P. Brand, J.P. Katstra, K. Sommerer, H.A. Stone, E. Nardell, G. Scheuch, Inhaling to mitigate exhaled bioaerosols, Proc. Natl. Acad. Sci. U. S. A. 101 (2004) 17383, https://doi.org/10.1073/pnas.0408159101. LP – 17388.

[19] F.B. Wurie, S.D. Lawn, H. Booth, P. Sonnenberg, A.C. Hayward, Bioaerosol production by patients with tuberculosis during normal tidal breathing: implications for transmission risk, Thorax 71 (2016) 549, https://doi.org/10.1136/thoraxjnl-2015-207295. LP – 554.

[20] D. Licina, G.C. Morrison, G. Bekö, C.J. Weschler, W.W. Nazaroff, Clothing-mediated exposures to chemicals and particles, Environ. Sci. Technol. 53 (2019) 5559–5575, https://doi.org/10.1021/acs.est.9b00272.

[21] J. Qian, J. Peccia, A.R. Ferro, Walking-induced particle resuspension in indoor environments, Atmos. Environ. 89 (2014) 464–481, https://doi.org/10.1016/j.atmosenv.2014.02.035.

[22] M. Täubel, H. Rintala, M. Pitkäranta, L. Paulin, S. Laitinen, J. Pekkanen, A. Hyvärinen, A. Nevalainen, The occupant as a source of house dust bacteria, J. Allergy Clin. Immunol. 124 (2009) 834–840, https://doi.org/10.1016/j.jaci.2009.07.045, e47.

[23] A.J. Prussin, L.C. Marr, Sources of airborne microorganisms in the built environment, Microbiome 3 (2015) 78, https://doi.org/10.1186/s40168-015-0144-z.

[24] A.M. Moldoveanu, Biological contamination of air in indoor spaces, in: Curr. Air Qual. Issues, IntechOpen, 2015, https://doi.org/10.5772/59727.

[25] J.M. Macher, F.-Y. Huang, M. Flores, A two-year study of microbiological indoor air quality in a new apartment, Arch. Environ. Health 46 (1991) 25–29, https://doi.org/10.1080/00039896.1991.9937425.

[26] N. Yamamoto, D. Hospodsky, K.C. Dannemiller, W.W. Nazaroff, J. Peccia, Indoor emissions as a primary source of airborne allergenic fungal particles in classrooms, Environ. Sci. Technol. 49 (2015) 5098–5106, https://doi.org/10.1021/es506165z.

[27] R.I. Adams, S. Bhangar, K.C. Dannemiller, J.A. Eisen, N. Fierer, J.A. Gilbert, J. L. Green, L.C. Marr, S.L. Miller, J.A. Siegel, B. Stephens, M.S. Waring, K. Bibby, Ten questions concerning the microbiomes of buildings, Build. Environ. 109 (2016) 224–234, https://doi.org/10.1016/j.buildenv.2016.09.001.

[28] B. Hanson, Y. Zhou, E.J. Bautista, B. Urch, M. Speck, F. Silverman, M. Muilenberg, W. Phipatanakul, G. Weinstock, E. Sodergren, D.R. Gold, J.E. Sordillo, Characterization of the bacterial and fungal microbiome in indoor dust and outdoor air samples: a pilot study, Environ. Sci. Process. Impacts. 18 (2016) 713–724, https://doi.org/10.1039/C5EM00639B.

[29] D. Hospodsky, N. Yamamoto, W.W. Nazaroff, D. Miller, S. Gorthala, J. Peccia, Characterizing airborne fungal and bacterial concentrations and emission rates in six occupied children's classrooms, Indoor Air 25 (2015) 641–652, https://doi.org/10.1111/ina.12172.

[30] D. Wilkins, M.H.Y. Leung, P.K.H. Lee, Indoor air bacterial communities in Hong Kong households assemble independently of occupant skin microbiomes, Environ. Microbiol. 18 (2016) 1754–1763, https://doi.org/10.1111/1462-2920.12889.

[31] A. Nevalainen, A. Hyvärinen, Chapter 9 - Fungi in Low-Contamination Occupational Environments, in: C. Viegas, A.C. Pinheiro, R. Sabino, S. Viegas,

J. Brandão, C. Veríssimo (Eds.), Academic Press, Amsterdam, 2016, pp. 107–125, https://doi.org/10.1016/B978-0-12-411471-5.00009-0.
[32] R.I. Adams, M. Miletto, J.W. Taylor, T.D. Bruns, The diversity and distribution of fungi on residential surfaces, PloS One 8 (2013), e78866, https://doi.org/10.1371/journal.pone.0078866.
[33] A. Nevalainen, M. Täubel, A. Hyvärinen, Indoor fungi: companions and contaminants, Indoor Air 25 (2015) 125–156, https://doi.org/10.1111/ina.12182.
[34] J. Qian, D. Hospodsky, N. Yamamoto, W.W. Nazaroff, J. Peccia, Size-resolved emission rates of airborne bacteria and fungi in an occupied classroom, Indoor Air 22 (2012) 339–351, https://doi.org/10.1111/j.1600-0668.2012.00769.x.
[35] D. Hospodsky, J. Qian, W.W. Nazaroff, N. Yamamoto, K. Bibby, H. Rismani-Yazdi, J. Peccia, Human occupancy as a source of indoor airborne bacteria, PloS One 7 (2012), e34867, https://doi.org/10.1371/journal.pone.0034867.
[36] D.N. Wagner, A. Mathur, B.E. Boor, Spatial seated occupancy detection in offices with a chair-based temperature sensor array, Build. Environ. 187 (2021) 107360, https://doi.org/10.1016/j.buildenv.2020.107360.
[37] N. Jung, S. Paiho, J. Shemeikka, R. Lahdelma, M. Airaksinen, Energy performance analysis of an office building in three climate zones, Energy Build. 158 (2018) 1023–1035, https://doi.org/10.1016/j.enbuild.2017.10.030.
[38] J. Jiang, N. Jung, B.E. Boor, Using building energy and smart thermostat data to evaluate indoor ultrafine particle source and loss processes in a net-zero energy house, ACS ES&T Eng. 1 (2021) 780–793, https://doi.org/10.1021/acsestengg.1c00002.
[39] C.H. Jasmine, S. Joel, Populations and determinants of airborne fungi in large office buildings, Environ. Health Perspect. 110 (2002) 777–782, https://doi.org/10.1289/ehp.02110777.
[40] K.M. Hewitt, C.P. Gerba, S.L. Maxwell, S.T. Kelley, Office space bacterial abundance and diversity in three metropolitan areas, PloS One 7 (2012), e37849, https://doi.org/10.1371/journal.pone.0037849.
[41] M. Gołofit-Szymczak, R.L. Górny, Microbiological air quality in office buildings equipped with dventilation systems, Indoor Air 28 (2018) 792–805, https://doi.org/10.1111/ina.12495.
[42] J. Chase, J. Fouquier, M. Zare, D.L. Sonderegger, R. Knight, S.T. Kelley, J. Siegel, J. G. Caporaso, Geography and location are the primary drivers of office microbiome composition, mSystems 1 (2016), https://doi.org/10.1128/mSystems.00022-16 e00022-16.
[43] A.K.Y. Law, C.K. Chau, G.Y.S. Chan, Characteristics of bioaerosol profile in office buildings in Hong Kong, Build. Environ. 36 (2001) 527–541, https://doi.org/10.1016/S0360-1323(00)00020-2.
[44] J.A. Huffman, A.E. Perring, N.J. Savage, B. Clot, B. Crouzy, F. Tummon, O. Shoshanim, B. Damit, J. Schneider, V. Sivaprakasam, M.A. Zawadowicz, I. Crawford, M. Gallagher, D. Topping, D.C. Doughty, S.C. Hill, Y. Pan, Real-time sensing of bioaerosols: review and current perspectives, Aerosol Sci. Technol. 54 (2020) 465–495, https://doi.org/10.1080/02786826.2019.1664724.
[45] M.J. Fennelly, G. Sewell, M.B. Prentice, D.J. O'Connor, J.R. Sodeau, Review: the use of real-time fluorescence instrumentation to monitor ambient primary biological aerosol particles (PBAP), Atmosphere 9 (2018), https://doi.org/10.3390/atmos9010001.
[46] J.A. Huffman, J. Santarpia, Online techniques for quantification and characterization of biological aerosols, Microbiol. Aerosols (2017) 83–114, https://doi.org/10.1002/9781119132318.ch1d.
[47] M. V Santander, B.A. Mitts, M.A. Pendergraft, J. Dinasquet, C. Lee, A.N. Moore, L. B. Cancelada, K.A. Kimble, F. Malfatti, K.A. Prather, Tandem fluorescence measurements of organic matter and bacteria released in sea spray aerosols, Environ. Sci. Technol. (2021), https://doi.org/10.1021/acs.est.0c05493.
[48] B. Cheng, S. Yue, W. Hu, L. Ren, J. Deng, L. Wu, P. Fu, Summertime fluorescent bioaerosol particles in the coastal megacity Tianjin, North China, Sci. Total Environ. 723 (2020) 137966, https://doi.org/10.1016/j.scitotenv.2020.137966.
[49] C.J. Schumacher, C. Pöhlker, P. Aalto, V. Hiltunen, T. Petäjä, M. Kulmala, U. Pöschl, J.A. Huffman, Seasonal cycles of fluorescent biological aerosol particles in boreal and semi-arid forests of Finland and Colorado, Atmos. Chem. Phys. 13 (2013) 11987–12001, https://doi.org/10.5194/acp-13-11987-2013.
[50] M.S.E. Toprak, Real Time Detection of Primary Biological Aerosol Particles (PBAP) in the Context of Atmospheric Ice Formation, Karlsruhe Institute of Technology, 2014. Ph.D. Dissertation.
[51] A.M. Gabey, M.W. Gallagher, J. Whitehead, J.R. Dorsey, P.H. Kaye, W.R. Stanley, Measurements and comparison of primary biological aerosol above and below a tropical forest canopy using a dual channel fluorescence spectrometer, Atmos. Chem. Phys. 10 (2010) 4453–4466, https://doi.org/10.5194/acp-10-4453-2010.
[52] A.E. Perring, J.P. Schwarz, D. Baumgardner, M.T. Hernandez, D. V Spracklen, C. L. Heald, R.S. Gao, G. Kok, G.R. McMeeking, J.B. McQuaid, D.W. Fahey, Airborne observations of regional variation in fluorescent aerosol across the United States, J. Geophys. Res. Atmos. 120 (2015) 1153–1170, https://doi.org/10.1002/2014JD022495.
[53] J. Li, M.P. Wan, S. Schiavon, K.W. Tham, S. Zuraimi, J. Xiong, M. Fang, E. Gall, Size-resolved dynamics of indoor and outdoor fluorescent biological aerosol particles in a bedroom: a one-month case study in Singapore, Indoor Air 30 (2020) 942–954, https://doi.org/10.1111/ina.12678.
[54] S. Bhangar, J.A. Huffman, W.W. Nazaroff, Size-resolved fluorescent biological aerosol particle concentrations and occupant emissions in a university classroom, Indoor Air 24 (2014) 604–617, https://doi.org/10.1111/ina.12111.
[55] M.L. Pereira, L.D. Knibbs, C. He, P. Grzybowski, G.R. Johnson, J.A. Huffman, S. C. Bell, C.E. Wainwright, D.L. Matte, F.H. Dominski, A. Andrade, L. Morawska, Sources and dynamics of fluorescent particles in hospitals, Indoor Air 27 (2017) 988–1000, https://doi.org/10.1111/ina.12380.
[56] Y. Tian, C. Arata, E. Boedicker, D.M. Lunderberg, S. Patel, S. Sankhyan, K. Kristensen, P.K. Misztal, D.K. Farmer, M. Vance, A. Novoselac, W.W. Nazaroff, A.H. Goldstein, Indoor emissions of total and fluorescent supermicron particles during HOMEChem, Indoor Air 31 (2021) 88–98, https://doi.org/10.1111/ina.12731.
[57] Y. Tian, Y. Liu, P.K. Misztal, J. Xiong, C.M. Arata, A.H. Goldstein, W.W. Nazaroff, Fluorescent biological aerosol particles: concentrations, emissions, and exposures in a northern California residence, Indoor Air 28 (2018) 559–571, https://doi.org/10.1111/ina.12461.
[58] Y. Xie, O.A. Fajardo, W. Yan, B. Zhao, J. Jiang, Six-day measurement of size-resolved indoor fluorescent bioaerosols of outdoor origin in an office, Particuology 31 (2017) 161–169, https://doi.org/10.1016/j.partic.2016.09.004.
[59] J. Li, L. Zhou, X. Zhang, C. Xu, L. Dong, M. Yao, Bioaerosol emissions and detection of airborne antibiotic resistance genes from a wastewater treatment plant, Atmos. Environ. 124 (2016) 404–412, https://doi.org/10.1016/j.atmosenv.2015.06.030.
[60] D. Lai, P. Karava, Q. Chen, Study of outdoor ozone penetration into buildings through ventilation and infiltration, Build. Environ. 93 (2015) 112–118, https://doi.org/10.1016/j.buildenv.2015.06.015.
[61] J. Kim, A. Tzempelikos, J.E. Braun, Energy savings potential of passive chilled beams vs air systems in various US climatic zones with different system configurations, Energy Build. 186 (2019) 244–260, https://doi.org/10.1016/j.enbuild.2019.01.031.
[62] D.J. O'Connor, D.A. Healy, S. Hellebust, J.T.M. Buters, J.R. Sodeau, Using the WIBS-4 (waveband integrated bioaerosol sensor) technique for the on-line detection of pollen grains, Aerosol Sci. Technol. 48 (2014) 341–349, https://doi.org/10.1080/02786826.2013.872768.
[63] D.A. Healy, D.J. O'Connor, J.R. Sodeau, Measurement of the particle counting efficiency of the "Waveband Integrated Bioaerosol Sensor" model number 4 (WIBS-4), J. Aerosol Sci. 47 (2012) 94–99, https://doi.org/10.1016/j.jaerosci.2012.01.003.
[64] A.I. Calvo, D. Baumgardner, A. Castro, D. Fernández-González, A.M. Vega-Maray, R.M. Valencia-Barrera, F. Oduber, C. Blanco-Alegre, R. Fraile, Daily behavior of urban fluorescing aerosol particles in northwest Spain, Atmos. Environ. 184 (2018) 262–277, https://doi.org/10.1016/j.atmosenv.2018.04.027.
[65] N.J. Savage, C.E. Krentz, T. Könemann, T.T. Han, G. Mainelis, C. Pöhlker, J. A. Huffman, Systematic characterization and fluorescence threshold strategies for the wideband integrated bioaerosol sensor (WIBS) using size-resolved biological and interfering particles, Atmos. Meas. Tech. 10 (2017) 4279–4302, https://doi.org/10.5194/amt-10-4279-2017.
[66] S.S. Patra, R. Ramsisaria, R. Du, T. Wu, B.E. Boor, A machine learning field calibration method for improving the performance of low-cost particle sensors, Build. Environ. 190 (2021) 107457, https://doi.org/10.1016/j.buildenv.2020.107457.
[67] J. Kim, J.E. Braun, A. Tzempelikos, W.T. Horton, Performance evaluation of a passive chilled beam system and comparison with a conventional air system, in: International High Performance Buildings Conference, 2016.
[68] J. Joe, P. Karava, X. Hou, J. Hu, Model predictive control of a radiant floor cooling system in an office space, in: International High Performance Buildings Conference, 2016.
[69] S. Li, J. Joe, J. Hu, P. Karava, System identification and model-predictive control of office buildings with integrated photovoltaic-thermal collectors, radiant floor heating and active thermal storage, Sol. Energy 113 (2015) 139–157, https://doi.org/10.1016/j.solener.2014.11.024.
[70] K.J. Heo, C.E. Lim, H.B. Kim, B.U. Lee, Effects of human activities on concentrations of culturable bioaerosols in indoor air environments, J. Aerosol Sci. 104 (2017) 58–65, https://doi.org/10.1016/j.jaerosci.2016.11.008.
[71] A.C.K. Lai, W.W. Nazaroff, Modeling indoor particle deposition from turbulent flow onto smooth surfaces, J. Aerosol Sci. 31 (2000) 463–476, https://doi.org/10.1016/S0021-8502(99)00536-4.
[72] W.W. Nazaroff, Indoor bioaerosol dynamics, Indoor Air 26 (2016) 61–78, https://doi.org/10.1111/ina.12174.
[73] P. Azimi, B. Stephens, HVAC filtration for controlling infectious airborne disease transmission in indoor environments: predicting risk reductions and operational costs, Build. Environ. 70 (2013) 150–160, https://doi.org/10.1016/j.buildenv.2013.08.025.
[74] R.L. Corsi, J.A. Siegel, C. Chiang, Particle resuspension during the use of vacuum cleaners on residential carpet, J. Occup. Environ. Hyg. 5 (2008) 232–238, https://doi.org/10.1080/15459620801901165.
[75] J. Zhou, W. Fang, Q. Cao, L. Yang, V.W.-C. Chang, W.W. Nazaroff, Influence of moisturizer and relative humidity on human emissions of fluorescent biological aerosol particles, Indoor Air 27 (2017) 587–598, https://doi.org/10.1111/ina.12349.
[76] S.W. Kembel, J.F. Meadow, T.K. O'Connor, G. Mhuireach, D. Northcutt, J. Kline, M. Moriyama, G.Z. Brown, B.J.M. Bohannan, J.L. Green, Architectural design drives the biogeography of indoor bacterial communities, PloS One 9 (2014), e87093, https://doi.org/10.1371/journal.pone.0087093.
[77] J. Li, W. Xu, Z. Li, M. Duan, B. Ouyang, S. Zhou, L. Lei, Y. He, J. Sun, Z. Wang, L. Du, Y. Sun, Real-time characterization of aerosol particle composition, sources and influences of increased ventilation and humidity in an office, Indoor Air (2021), https://doi.org/10.1111/ina.12838 n/a.
[78] P. Azimi, D. Zhao, B. Stephens, Estimates of HVAC filtration efficiency for fine and ultrafine particles of outdoor origin, Atmos. Environ. 98 (2014) 337–346, https://doi.org/10.1016/j.atmosenv.2014.09.007.
[79] S. Asadi, A.S. Wexler, C.D. Cappa, S. Barreda, N.M. Bouvier, W.D. Ristenpart, Aerosol emission and superemission during human speech increase with voice loudness, Sci. Rep. 9 (2019) 2348, https://doi.org/10.1038/s41598-019-38808-z.

[80] M. Alsved, A. Matamis, R. Bohlin, M. Richter, P.-E. Bengtsson, C.-J. Fraenkel, P. Medstrand, J. Löndahl, Exhaled respiratory particles during singing and talking, Aerosol Sci. Technol. 54 (2020) 1245–1248, https://doi.org/10.1080/02786826.2020.1812502.

[81] C.A. Mackintosh, O.M. Lidwell, A.G. Towers, R.R. Marples, The dimensions of skin fragments dispersed into the air during activity, J. Hyg. 81 (1978) 471–480, https://doi.org/10.1017/S0022172400025341.

[82] K. Findley, J. Oh, J. Yang, S. Conlan, C. Deming, J.A. Meyer, D. Schoenfeld, E. Nomicos, M. Park, J. Becker, B. Benjamin, R. Blakesley, G. Bouffard, S. Brooks, H. Coleman, M. Dekhtyar, M. Gregory, X. Guan, J. Gupta, J. Han, A. Hargrove, S. Ho, T. Johnson, R. Legaspi, S. Lovett, Q. Maduro, C. Masiello, B. Maskeri, J. McDowell, C. Montemayor, J. Mullikin, M. Park, N. Riebow, K. Schandler, B. Schmidt, C. Sison, M. Stantripop, J. Thomas, P. Thomas, M. Vemulapalli, A. Young, H.H. Kong, J.A. Segre, Topographic diversity of fungal and bacterial communities in human skin, Nature 498 (2013) 367–370, https://doi.org/10.1038/nature12171.

[83] A.M. Cundell, Microbial ecology of the human skin, Microb. Ecol. 76 (2018) 113–120, https://doi.org/10.1007/s00248-016-0789-6.

[84] E.A. Grice, H.H. Kong, G. Renaud, A.C. Young, G.G. Bouffard, R.W. Blakesley, T. G. Wolfsberg, M.L. Turner, J.A. Segre, A diversity profile of the human skin microbiota, Genome Res. 18 (2008) 1043–1050, https://doi.org/10.1101/gr.075549.107.

[85] Y.H. Yoon, P. Brimblecombe, Clothing as a source of fibres within museums, J. Cult. Herit. 1 (2000) 445–454, https://doi.org/10.1016/S1296-2074(00)01099-2.

[86] M. Hernandez, A.E. Perring, K. McCabe, G. Kok, G. Granger, D. Baumgardner, Chamber catalogues of optical and fluorescent signatures distinguish bioaerosol classes, Atmos. Meas. Tech. 9 (2016) 3283–3292, https://doi.org/10.5194/amt-9-3283-2016.

[87] A.W. Burg, M.W. Rohovsky, C.J. Kensler, G.N. Wogan, Current status of human safety and environmental aspects of fluorescent whitening agents used in detergents in the United States, C R C Crit, Rev. Environ. Control. 7 (1977) 91–120, https://doi.org/10.1080/10643387709381648.

[88] I. Crawford, M.W. Gallagher, K.N. Bower, T.W. Choularton, M.J. Flynn, S. Ruske, C. Listowski, N. Brough, T. Lachlan-Cope, Z.L. Fleming, V.E. Foot, W.R. Stanley, Real-time detection of airborne fluorescent bioparticles in Antarctica, Atmos. Chem. Phys. 17 (2017) 14291–14307, https://doi.org/10.5194/acp-17-14291-2017.

[89] I. Crawford, G. Lloyd, E. Herrmann, C.R. Hoyle, K.N. Bower, P.J. Connolly, M. J. Flynn, P.H. Kaye, T.W. Choularton, M.W. Gallagher, Observations of fluorescent aerosol–cloud interactions in the free troposphere at the High-Altitude Research Station Jungfraujoch, Atmos. Chem. Phys. 16 (2016) 2273–2284, https://doi.org/10.5194/acp-16-2273-2016.

[90] M.I. Gosselin, C.M. Rathnayake, I. Crawford, C. Pöhlker, J. Fröhlich-Nowoisky, B. Schmer, V.R. Després, G. Engling, M. Gallagher, E. Stone, U. Pöschl, J. A. Huffman, Fluorescent bioaerosol particle, molecular tracer, and fungal spore concentrations during dry and rainy periods in a semi-arid forest, Atmos. Chem. Phys. 16 (2016) 15165–15184, https://doi.org/10.5194/acp-16-15165-2016.

[91] N.J. Savage, J.A. Huffman, Evaluation of a hierarchical agglomerative clustering method applied to WIBS laboratory data for improved discrimination of biological particles by comparing data preparation techniques, Atmos. Meas. Tech. 11 (2018) 4929–4942, https://doi.org/10.5194/amt-11-4929-2018.